Institute for Environment and Sustainability

joint research centre
EUROPEAN COMMISSION

Calibration of the LISFLOOD model for Europe: current status and way forward

Luc Feyen

EUROPEAN COMMISSION
DIRECTORATE-GENERAL
Joint Research Centre

2005 **EUR 22125 EN**

Printed in Italy

Abstract

The hydrological model LISFLOOD model forms the core of the European Flood Alert System (EFAS) and is used for impact studies to evaluate the effect of changes in land use and climate on the hydrological behaviour in catchments across Europe. The accuracy of the model predictions depends on the ability of the model to capture the dominating hydrological processes that transfer precipitation into river runoff at the catchment scale, and on its ability to reproduce historical time series of observed river discharges. A crucial step which contributes significantly to the accuracy of the LISFLOOD forecasts and simulations is the calibration of the model for all European catchments. Owing to the general nature of LISFLOOD, its application to any given river basin requires that certain parameters of conceptual functions be identified for the particular basin. An automatic calibration procedure has been developed for LISFLOOD, based on the Shuffled Complex Evolution Metropolis (SCEM-UA) global optimization algorithm [Vrugt et al., 2003]. The algorithm automatically searches through the space of feasible parameter values and finds the parameter values that produce the best model performance. It also yields a posterior parameter distribution, which reflects the residual uncertainty about the model parameters after taking into account the discharge observations. The posterior distribution forms the basis for making probabilistic flow predictions. To overcome the computational burden the optimization has been implemented using parallel computing. This document outlines the automatic calibration method and shows results for the Meuse and Morave catchments.

Content

1. General situation of the problem ---------- 8
2. Automatic calibration of the LISFLOOD model employing the Shuffled Complex Evolution Metropolis (SCEM-UA) algorithm ---------- 9
   2.1. Bayesian framework for hydrological parameter estimation ---------- 10
   2.2. Shuffled Complex Evolution Metropolis Algorithm ---------- 12
   2.3. Implementation of SCEM-UA using parallel computing ---------- 14
   2.4. Model parameterisation ---------- 16
3. Calibration results ---------- 18
   3.1. Uniform parameter calibration for the Meuse catchment ---------- 18
   3.2. Semi-distributed calibration for the Morava catchment ---------- 29
4. Conclusions ---------- 41
5. Further work ---------- 42

References ---------- 43

1. General situation of the problem

The hydrological model LISFLOOD [De Roo et al., 2000; 2001] model forms the core of the European Flood Alert System (EFAS) and is used for impact studies to evaluate the effect of changes in land use and climate on the hydrological behaviour in catchments across Europe. LISFLOOD is a spatially distributed, partly physically-based hydrological model embedded within a PCRaster GIS environment. The model simulates river discharges in drainage basins as a function of spatial information on topography, soils and land cover. The accuracy of the model predictions depends on the ability of the model to capture the dominating hydrological processes that transfer precipitation into river runoff at the catchment scale, and on its ability to reproduce historical time series of observed river discharges.

A crucial step which contributes significantly to the accuracy of the LISFLOOD forecasts and simulations is the calibration of the model for all European catchments. Owing to the general nature of LISFLOOD, its application to any given river basin requires that certain parameters of conceptual functions be identified for the particular basin. In the process of calibration, the values of unknown model parameters are tuned such that the model matches the observed predictions as closely as possible.

During the early stages of the EFAS project, the LISFLOOD model has been crudely calibrated, without taking due account of the spatial variability of the parameters over the different hydrological regimes across Europe. A set of 240 parameters realizations was generated, and for large catchments the parameter set was chosen that best reproduced a time series of observed river discharges at the outlet. For ungauged catchments the parameter set that gave the best prediction in most other catchments was used. The underlying assumption was that the 240 parameter realizations were a representative sample of the feasible parameter space.

More recently, several detached national experts have been working on a more detailed calibration of the LISFLOOD model for the Danube and Elbe catchments, typically by manually adjusting the parameters while visually inspecting the agreement between the observed and simulated discharges. However, the subjective and time-consuming nature of the trial-and-error method renders this method unappealing for use at a European

scale. The large number of catchments for which the model needs to be calibrated calls for an automatic parameter estimation procedure. Besides shortening the implementation time this will also enhance the reliability of the calibrated parameters due to a more exhaustive exploration of the parameter space.

An automatic calibration procedure has been developed for LISFLOOD, based on the Shuffled Complex Evolution Metropolis (SCEM-UA) global optimization algorithm [Vrugt et al., 2003]. The algorithm automatically searches through the space of feasible parameter values and finds the parameter values that produce the best model performance. It also yields a posterior parameter distribution, which reflects the residual uncertainty about the model parameters after taking into account the discharge observations. The posterior distribution forms the basis for making probabilistic flow predictions. To overcome the computational burden the optimization has been implemented using parallel computing.

The work done on the calibration in 2005 resulted in one paper in the proceedings of the International Conference on Innovation, advances and implementation of flood forecasting technology in Tromsø [Feyen et al., 2005a], an oral presentation at the American Geophysical Union Fall Meeting in San Francisco [Feyen et al., 2005b], an article submitted to Journal of Hydrology [Feyen et al., 2006a], and a manuscript in preparation [Feyen et al., 2006b].

The aim of this document is to provide an overview and some results of the calibration work of the LISFLOOD model that has been carried out during 2005. The document is organised as follows. Section 2 provides details about the automatic calibration procedure and its implementation. Some results are presented in Section 3. Conclusions and further work can be found in Sections 4 and 5.

2. Automatic calibration of the LISFLOOD model employing the Shuffled Complex Evolution Metropolis (SCEM-UA) algorithm

This section describes the Bayesian inference method adopted for the calibration and parameter uncertainty assessment of the LISFLOOD rainfall-runoff model. First, a generic mathematical formulation of the Bayesian procedure for hydrological inversion

is provided. The second part of this section details the SCEM-UA optimisation code used to perform the computations. Details on the parallel implementation of SCEM-UA conclude the section.

In Bayesian inference knowledge and uncertainty about variables is summarised in probability distributions. In what follows, we use the notation $p(\ )$ for probability density functions, $L(\ )$ for likelihood functions, and a vertical bar to indicate conditioning. Arguments on the left side of the vertical bar denote the variables of the density; arguments on the right side of the bar denote the fixed values on which the density is conditioned.

2.1. Bayesian framework for hydrological parameter estimation

Calibration or inverse problems arise anywhere data are collected that are related to unknown quantities by a mathematical model. The unknown quantities here are the hydrological properties of the river basin under study (e.g., hydraulic properties of the soil, storage or surface routing properties), with the collected data given by observed responses of the system (e.g., river stage or discharge, soil moisture content, groundwater table elevation). The Bayesian approach to the non-linear calibration or inverse problem is the transfer of information from the observed system responses to the unknown quantities, hereby updating the probability density functions that describe the uncertainty about the unknown variables.

The functional form, here the non-linear hydrological model LISFLOOD, relating the system responses with the unknown quantities can be written as

$$\mathbf{y}_{\mathrm{F}} = \mathrm{F}(\boldsymbol{\theta}, \boldsymbol{\xi}) \tag{2.1}$$

where $\mathbf{y}_{\mathrm{F}} = (y_{\mathrm{F},1}, y_{\mathrm{F},2}, ..., y_{\mathrm{F},n_y})^{\mathrm{T}}$ is the functional output, $\boldsymbol{\theta} \in \Theta \subset \Re^{n_\theta}$ is the vector of model parameters representing the unknown hydrological river basin properties, and $\boldsymbol{\xi} \in \Xi \subset \Re^{n_\xi}$ comprises the forcing inputs to the hydrological model, such as precipitation or ET_0 rates, recharge or discharge fluxes at boundaries, and withdrawal/injection rates.

Omitting from the notation the inputs $\boldsymbol{\xi}$ to the hydrological model that are assumed to be known and fixed, the relation between the observed system responses $\mathbf{y} = (y_1, y_2, ..., y_{n_y})^{\mathrm{T}}$ and the model predictions is given by

$$\mathbf{y} = \mathbf{y}_{\mathrm{F}} + \boldsymbol{\varepsilon}_y(\boldsymbol{\theta}) \tag{2.2}$$

where $\boldsymbol{\varepsilon}_y = (\varepsilon_{y,1}, \varepsilon_{y,2}, ..., \varepsilon_{y,n_y})^{\mathrm{T}}$ is the vector of modelling residuals, which contains various sources of potential prediction errors. The functions we employ, even the most elaborate physically-based models, cannot reflect the true complexity and are necessarily simplifications of the processes occurring in the field. Aggregation and lumping of processes in space and time leads to parameter identification errors. Also, observations of system responses are prone to measurement errors.

To implement Bayesian inference, a probability density function with parameters $\boldsymbol{\psi} \in \Psi \subset \Re^{n_\psi}$ needs to be specified for the residuals that is consistent with the available information about the errors. The joint conditional distribution $p(\boldsymbol{\varepsilon}_y | \boldsymbol{\theta}, \boldsymbol{\psi})$ describes the distribution of the residuals, given $\boldsymbol{\theta}$ and the parameters $\boldsymbol{\psi}$ of the assumed error model. This expression, seen as a function of $\boldsymbol{\theta}$ and $\boldsymbol{\psi}$, is called the likelihood function, and expresses the likelihood of observing the residuals given $\boldsymbol{\theta}$ and $\boldsymbol{\psi}$. Since the structure of $\mathrm{F}(\boldsymbol{\theta})$ is known, the likelihood function is actually proportional to the probability distribution of the observed system responses, i.e., $L(\boldsymbol{\theta}, \boldsymbol{\psi} | \mathbf{y}) \equiv p(\mathbf{y} | \boldsymbol{\theta}, \boldsymbol{\psi})$. Parameter values that closely reproduce the observed system responses will be characterised by high likelihood values.

The information contained in the observed system responses, by means of the likelihood function $L(\boldsymbol{\theta}, \boldsymbol{\psi} | \mathbf{y})$, is used to update the prior information of the parameters $\boldsymbol{\theta}$, expressed by the prior distribution $p(\boldsymbol{\theta})$, and the prior information about the error model, expressed by the prior distribution $p(\boldsymbol{\psi})$. The prior distributions may be defined based on other data sets or a modeller's experience and physical intuition. Assuming conditional independence between $p(\boldsymbol{\theta})$ and $p(\boldsymbol{\psi})$, Bayes' theorem gives

$$p(\boldsymbol{\theta}, \boldsymbol{\psi}|\mathbf{y}) = C_y^{-1}\, L(\boldsymbol{\theta}, \boldsymbol{\psi}|\mathbf{y})\; p(\boldsymbol{\theta})\; p(\boldsymbol{\psi}) \tag{2.3}$$

where $C_y = \int_{\Theta}\int_{\Psi} L(\boldsymbol{\theta}, \boldsymbol{\psi}|\mathbf{y})\; p(\boldsymbol{\theta})\; p(\boldsymbol{\psi}) \partial\boldsymbol{\theta}\, \partial\boldsymbol{\psi}$ is the normalising constant, provided the integral exists.

The marginal posterior distribution $p(\boldsymbol{\theta}|\mathbf{y})$ is then obtained by integrating the joint posterior distribution $p(\boldsymbol{\theta}, \boldsymbol{\psi}|\mathbf{y})$ over the nuisance parameters $\boldsymbol{\psi}$ of the error model

$$p(\boldsymbol{\theta}|\mathbf{y}) = \int_{\Psi} p(\boldsymbol{\theta}, \boldsymbol{\psi}|\mathbf{y})\, \partial\boldsymbol{\psi} \tag{2.4}$$

The conditional distribution $p(\boldsymbol{\theta}|\mathbf{y})$ reflects the uncertainty about the model parameters after the observations of the system responses have been considered. It forms the basis for making predictions about the system responses with the model. For any future time step t_i the predictive distribution of the system responses is then given by the expression

$$p(\mathbf{y}_{t_i}|\mathbf{y}) = \int_{\Theta} p(\mathbf{y}_{t_i}|\mathbf{y}, \boldsymbol{\theta})\; p(\boldsymbol{\theta}|\mathbf{y})\, \partial\boldsymbol{\theta} \tag{2.5}$$

Summarising statistics about the flow predictions, such as measures of the central tendency or spread, or the probability of exceeding a user-defined threshold, are readily obtained from this probability density function.

2.2. Shuffled Complex Evolution Metropolis Algorithm

Typically, for hydrological problems the joint posterior parameter distribution $p(\boldsymbol{\theta}|\mathbf{y})$ is highly dimensional and complex, with strong non-linear parameter interdependences. Hence, $p(\boldsymbol{\theta}|\mathbf{y})$ is not easily amenable to direct sampling or analytical integration and it is necessary to resort to Monte Carlo methods to approximate the distribution. Since we do not know the form of the joint posterior distribution in our context, we adopt a Markov Chain Monte Carlo (MCMC) approach to compute $p(\boldsymbol{\theta}|\mathbf{y})$. In particular, we

employ the Shuffled Complex Evolution Metropolis (SCEM-UA) algorithm [Vrugt et al., 2003], which uses the Metropolis-Hastings [Metropolis et al., 1953; Hastings, 1970] search strategy to generate a sequence of parameter sets $\{\boldsymbol{\theta}_1, \boldsymbol{\theta}_2, ..., \boldsymbol{\theta}_n\}$ that adapts to the target posterior distribution.

The SCEM-UA algorithm starts with generating an initial population of s parameter sets sampled from the joint prior parameter distribution $p(\boldsymbol{\theta})$. The latter constrains the parameter space and represents the belief about the parameters before any data are collected. Independent uniform prior parameter distributions between realistic lower and upper bounds are typically adopted for each parameter in $\boldsymbol{\theta}$. This implies that the information in the data, expressed by the likelihood function, should dominate the form of the resulting posterior distribution. Note that the assumption of prior independence among the parameters is by no means necessary and can be relaxed only at the cost of making computations more burdensome.

Assuming that the residuals $\boldsymbol{\varepsilon}_y = (\varepsilon_{y,1}, \varepsilon_{y,2}, ..., \varepsilon_{y,n_y})^{\mathrm{T}}$ are mutually independent, normally distributed with a constant variance σ_ε, the likelihood of each parameter set $\boldsymbol{\theta}$ given the observations $\mathbf{y}$ is computed using [Box and Tiao, 1973]

$$L(\boldsymbol{\theta}, \boldsymbol{\psi}|\mathbf{y}) = \exp\left[-\frac{1}{2} \sum_{i=1}^{n_y} \left| \frac{\upsilon_i(\boldsymbol{\theta})}{\sigma_\varepsilon} \right|^2 \right] \tag{2.6}$$

where

$$\upsilon_i(\boldsymbol{\theta}) = G(y_{F,i}) - G(y_i) \tag{2.7}$$

The transformation $G(.)$ of the simulated and observed system responses allows to handle non-normality, lack of variance homogeneity and autocorrelation of error terms in the residuals. The parameter of the error model, i.e., $\boldsymbol{\psi} = \sigma_\varepsilon$, is treated as a hyperparameter whose uncertainty is accounted for by marginalisation. Assuming a non-informative prior $p(\sigma_\varepsilon) \sim 1/\sigma_\varepsilon$, and given the uniform prior parameter

distributions adopted, the posterior density for each parameter set $\boldsymbol{\theta}$ given the observations $\mathbf{y}$ is obtained using [Box and Tiao, 1973]

$$p(\boldsymbol{\theta}|\mathbf{y}) = C^{-1}\left[\sum_{i=1}^{N}\left|\upsilon_i(\boldsymbol{\theta})\right|^2\right]^{-\frac{1}{2}n_y} \tag{2.8}$$

where $C = \int\left[\sum_{i=1}^{N}\left|\upsilon_i(\boldsymbol{\theta})\right|^2\right]^{-\frac{1}{2}N}\delta\boldsymbol{\theta}$ is the normalising constant.

Once the posterior density has been computed for the s parameter combinations of the initial sample using (2.8), the population is partitioned into q complexes. In each complex a parallel sequence is launched from the point with the highest posterior density. New candidate points are generated employing a multivariate normal distribution centred around the current draw of the sequence or the mean of the points in the complex augmented with the covariance structure induced between the points in the complex. Equation (2.8) is used to compute the posterior density of new candidate points, which are added (by random replacement) to the current sequence based on the Metropolis-annealing [Metropolis et al., 1953] criterion. After a predefined number of iterations the complexes are shuffled to share information gained independently in the parallel sequences. This series of operations yields a robust MCMC sampler that efficiently and effectively searches the parameter space and converges to the target distribution for a sufficiently large number of iterations (typically > 2,500 iterations).

2.3. Implementation of SCEM-UA using parallel computing

Due to the computational demands of the LISFLOOD model and the large number of iterations typically needed to obtain a stable posterior parameter distribution it was required to implement the SCEM-UA algorithm using parallel computing. We employed a LAM/MPI distributed computing interface for the Octave programming environment [Vrugt et al., 2005]. LAM/MPI is a high-quality open-source implementation of the Message Passing Interface specification that includes a rich set of features for parallel computing. GNU Octave [Eaton, 1998; 2001] is a high-level language, compatible with MATLAB^{TM}, that is intended primarily for numerical

computations. It provides a convenient command line interface for the numerical solution of linear and nonlinear problems, and for performing numerical experiments. A detailed description and explanation of the software appear in Fernández et al. [2003, 2004]. The parallel implementation scheme of the SCEM-UA algorithm is presented in Figure 2.1. For the calibration of the 5 km Meuse catchment upstream of Borgharen (approximately 22.000 km^2) the calculations were performed using 11 Pentium IV 3.40 GHz processors of the LISA cluster belonging to the SARA parallel computing centre (the Netherlands). The CPU time required for the stochastic calibration of the LISFLOOD model for a 3-year simulation period with a daily time step and 10.000 SCEM-UA generated parameters combinations was approximately 35 hours.

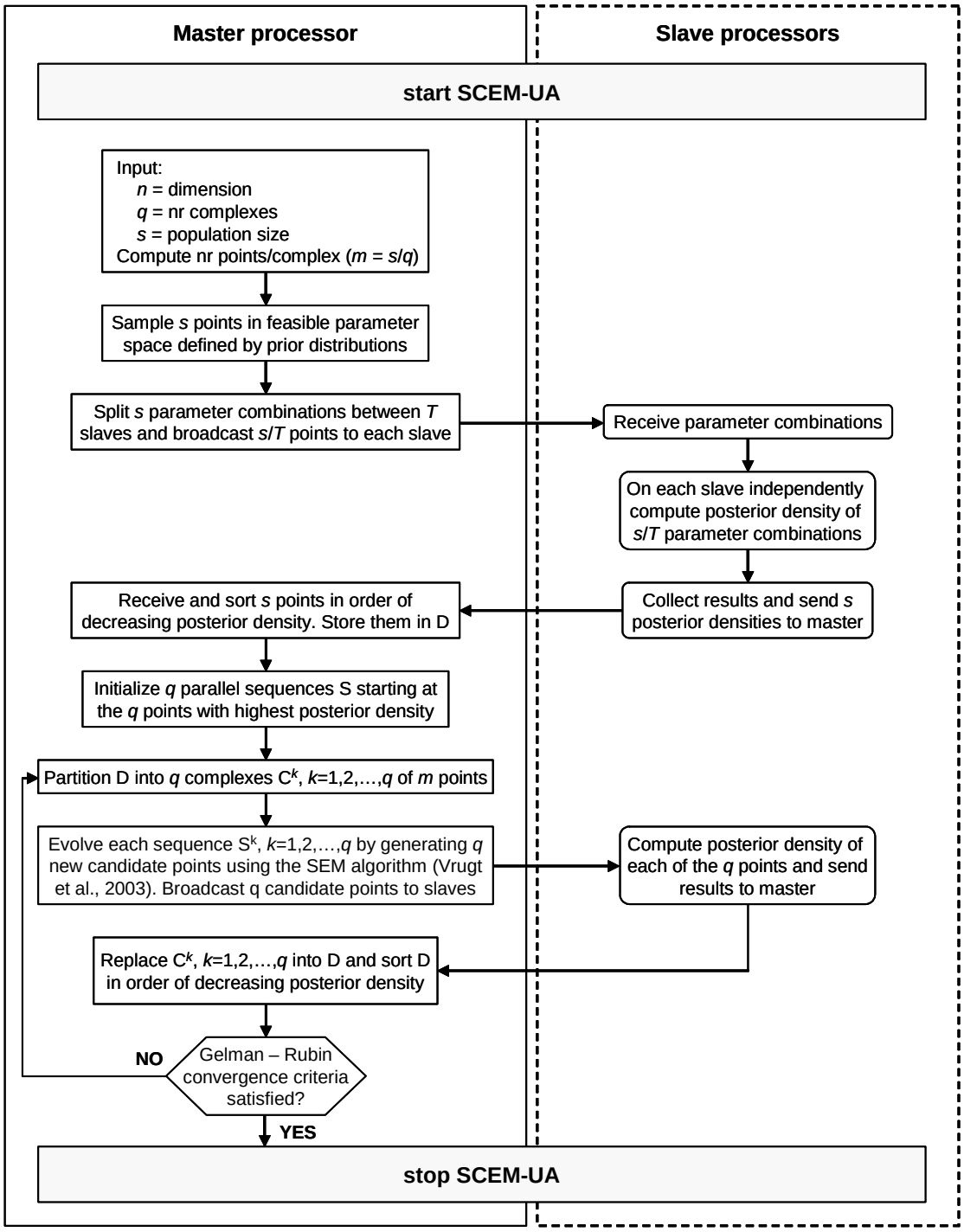

Figure 2.1. Flow chart of parallel implementation of SCEM-UA

2.4. Model parameterisation

Distributed models require a vast amount of data to represent the spatial distribution of the meteorological and hydrological characteristics of large river basins. A rigorous parameterisation procedure is crucial to avoid methodological problems during model calibration. Spatial patterns of the parameter values have to be specified such that

parameters reflect only significant and systematic spatial variations inherent in the available data. As such, the parameterisation process can effectively reduce the number of free parameters to be adjusted during calibration [Refsgaard, 1997].

To avoid problems of over-parameterisation and to reduce the dimensionality of the model calibration, input parameters and variables of LISFLOOD are estimated a priori from available data bases as much as possible. For example, soil physical properties are derived from the European Soil Geographical Database [King et al., 1994]. The HYPRES database [Wösten et al., 1999] is used to estimate porosity, saturated hydraulic conductivity and moisture retention properties for each texture class. Vegetation and land use information are obtained from the Corine land cover database [EEA, 2000]. Meteorological parameters are extracted from the MARS Meteorological Database. Digital elevation data are obtained from the Catchment Information System, which has a spatial resolution of 1 km [Hiederer and De Roo, 2003].

Although LISFLOOD is based on physics to a certain extent, some processes are only represented in a lumped conceptual way. As a result, some parameters lack physical basis and cannot be directly obtained from field data. In the current version of LISFLOOD, there remain five parameters that need to be estimated by calibration against measured stream flow records. The calibration parameters are tabulated in Table 1, with the upper and lower bounds of the prior distributions used in the inverse procedure. The Upper Zone Time Constant (UZTC) and Lower Zone Time Constant (LZTC) reflect the residence time of water in the upper and lower groundwater zone, respectively. As such, they control the amount and timing of outflow from the respective groundwater reservoirs. The Groundwater Percolation Value (GWPV) controls the flow from the upper to the lower groundwater zone. The Xinanjiang parameter b (Xb) is an empirical shape parameter in the Xinanjiang model [Zhao and Lui, 1995] that is used to simulate infiltration. In controls the fraction of saturated area within a grid cell that is contributing to runoff, hence it is inversely related to infiltration. The Power Preferential Bypass Flow parameter (PPBF) is an empirical shape parameter in the power function relating preferential flow with the relative saturation of the soil.

Table 2.1. Calibration parameters of the LISFLOOD model with upper and lower bounds of the prior uniform distributions.

Parameter	Lower bound	Upper bound
Upper Zone Time Constant (UZTC)	1	10
Lower Zone Time Constant (LZTC)	10	5000
Ground Water Percolation Value (GWPV)	0	0.5
Xinanjiang parameter b (Xb)	0.05	0.5
Power Preferential Bypass Flow (PPF)	5	15

3. Calibration results

So far, the automatic calibration procedure has been tested and implemented for several pilot basins, including catchments and subcatchments of the Meuse (both the 5 and 1 km model), the Saone, the Odra and the Danube. In this section some results are presented. The first part presents results for the Meuse (5 km model) catchment upstream of Borgharen, where the 5 calibration parameters were uniformly distributed over the catchment. In the second part, some results are presented about an exercise to evaluate the minimum level of spatial detail of the 5 unknown parameters for simulating river discharges in large-scale river basins.

3.1. Uniform parameter calibration for the Meuse catchment

Results are presented for the Meuse catchment upstream of Borgharen. This part of the Meuse catchment covers an area of approximately 21,000 km^2 and is situated in Belgium, France, and the Netherlands. The Meuse is fed mainly by rain all year round; hence flows are generally highest in winter, with relatively low flows during the summer. The topography of the area is hilly with the elevation varying from 50 m to 700 m. The substrata are largely impervious, resulting in precipitation that is discharged quickly into the river. The predominant land use types are forest, agriculture (cultivated patterns and pasture), moor and heath.

In the model, the area was discretised in 5 by 5 km grid blocks. Daily observed discharges are available for the Borgharen gauging station. The model was run with a daily time step. The simulation period in the calibration spanned 1/10/1992-30/09/1995.

The first year was used as a warming-up period, hence only predicted discharges for the last two years were used for the calibration. For validating the model, observations from 10/1/1990-30/9/1992 were used.

Several important assumptions underlie the use of 2.6 as a likelihood function in the derivation of the posterior parameter distribution, namely that the residuals are uncorrelated in time and normally distributed with constant variance. If these assumptions are not met, the posterior parameter distribution may not adequately describe parameter uncertainty, and the derived predictive uncertainty bounds may be erroneous. The transformation $G(.)$ in 2.7 of the simulated and observed system responses allows to handle non-normality, lack of variance homogeneity and autocorrelation of error terms in the residuals. In this work, we only account for non-normality and heteroscedastic errors by applying a Box-Cox transformation with $\lambda = 0.4$ to the observed and simulated discharge series. The validity of these assumptions is evaluated later in this section using diagnostic checks. Correlation of the residuals in time can be accounted for by fitting autoregressive (AR), moving average (MA) or mixed (ARMA) error models to the residuals [see e.g., Sorooshian and Dracup, 1980; Kuczera, 1983; Bates and Cambell, 2001].

The SCEM-UA algorithm was run with a population sizes $s = 250$ and $q = 10$ complexes, or 25 points in each complex. Convergence of the MCMC sampler to a stationary distribution was evaluated using the Scale Reduction score ($\sqrt{SR}$) defined by Gelman and Rubin [1992]. If the scale reduction score is less than 1.2, the Markov chain is considered to be converged; otherwise, more runs are needed. In Figure 3.1 calculated values of $\sqrt{SR}$ are plotted against the number of MCMC iterations. The line plots indicate that for all parameters the parallel sequences converged to the target distribution after approximately 3000 iterations.

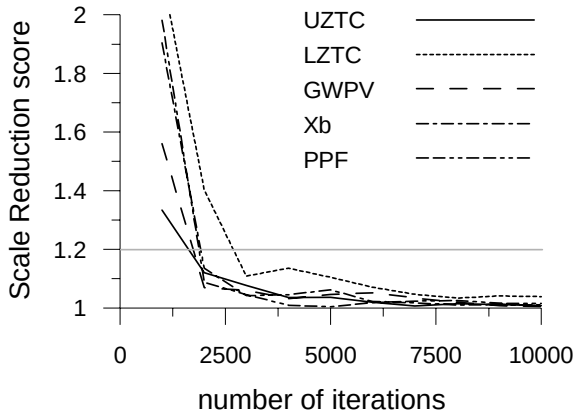

Figure 3.1. Evolution of the Gelman and Rubin Scale Reduction score for LISFLOOD calibration parameters

The rapid convergence is confirmed by the evolution of the samples generated in the q = 10 sequences presented in Figure 3.2. Initially, parameter values are sampled from the feasible parameter space defined by the prior parameter distributions. After this initial exploration of the parameter space, the sampler discards parameter regions with low posterior probabilities. For the UZTC, GWPV, Xb, and PPF parameters, the SCEM-algorithm rapidly occupies only a small range of the initial parameter ranges. For the LZTC no clear defined region of attraction exists.

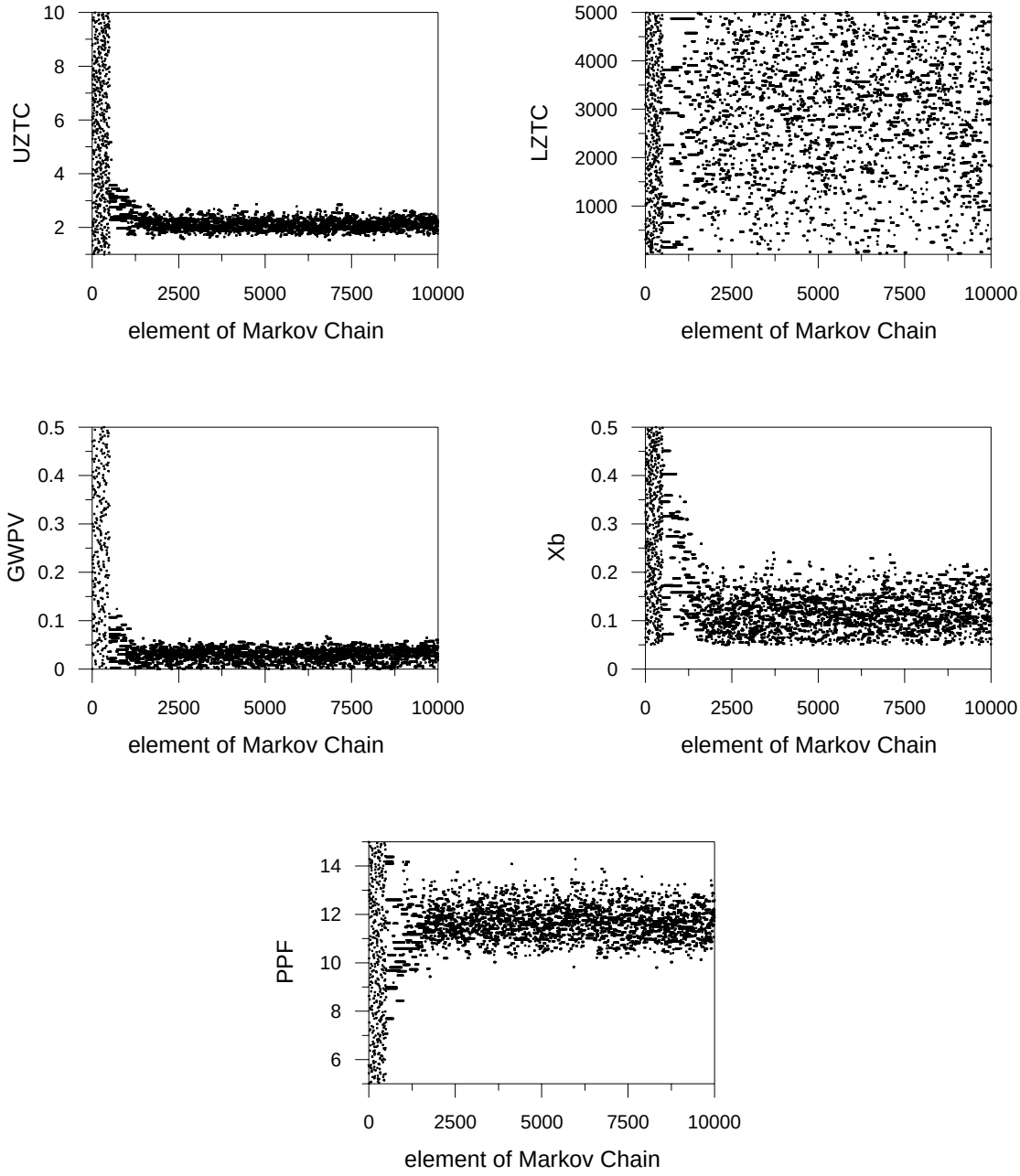

Figure 3.2. Markov Chain Monte Carlo samples generated in the q = 10 sequences for the LISFLOOD calibration parameters

Figure 3.3 presents the marginal posterior probability distributions for the LISFLOOD calibration parameters constructed using 7,000 samples generated after convergence of the SCEM-UA algorithm. Note that for all parameters but the LZTC the limits of the *x*-axis in Figure 3.6 do not correspond to the range specified for the respective prior uniform distributions. The summarizing statistics of the posterior parameter distributions together with the most likely parameter combination are presented in Table 3.1. The posterior density for the UZTC and PPF approximate a normal distribution

centred around the optimal parameter values; hence, the posterior mean is close to the optimal parameter value. The well defined region of small values for UZTC reflects the short residence times in the upper groundwater zone. This means that water that has passed the soil zone is quickly discharged into the river channel, which can be related to the impervious subsoil strata present in large parts of the catchment. The high values for the PPF indicate that the contribution of preferential flow bypassing the soil zone is only significant under wet conditions. For the Xb parameter the posterior density also approximates a normal distribution, but it is truncated at the lower boundary of the prior distribution. The low posterior values for the Xb parameter show that runoff in the catchment is small unless the soil is nearly fully saturated. The posterior density for the GWPV parameter is concentrated on very low values, indicating that the amount of flow from the upper to the lower groundwater zone is limited. Indeed, analysis of the different components contributing to the total discharge showed that the outflow of the lower groundwater zone only accounts for 1.6%. The nearly negligible contribution of the lower groundwater zone also explains the approximately flat response surface for the LZTC parameter. The posterior distributions and standard deviations depict that the calibration parameters of the LISFLOOD model, except for the lower zone time constant, are well identifiable for the Meuse catchment using 2 years of measured daily discharges.

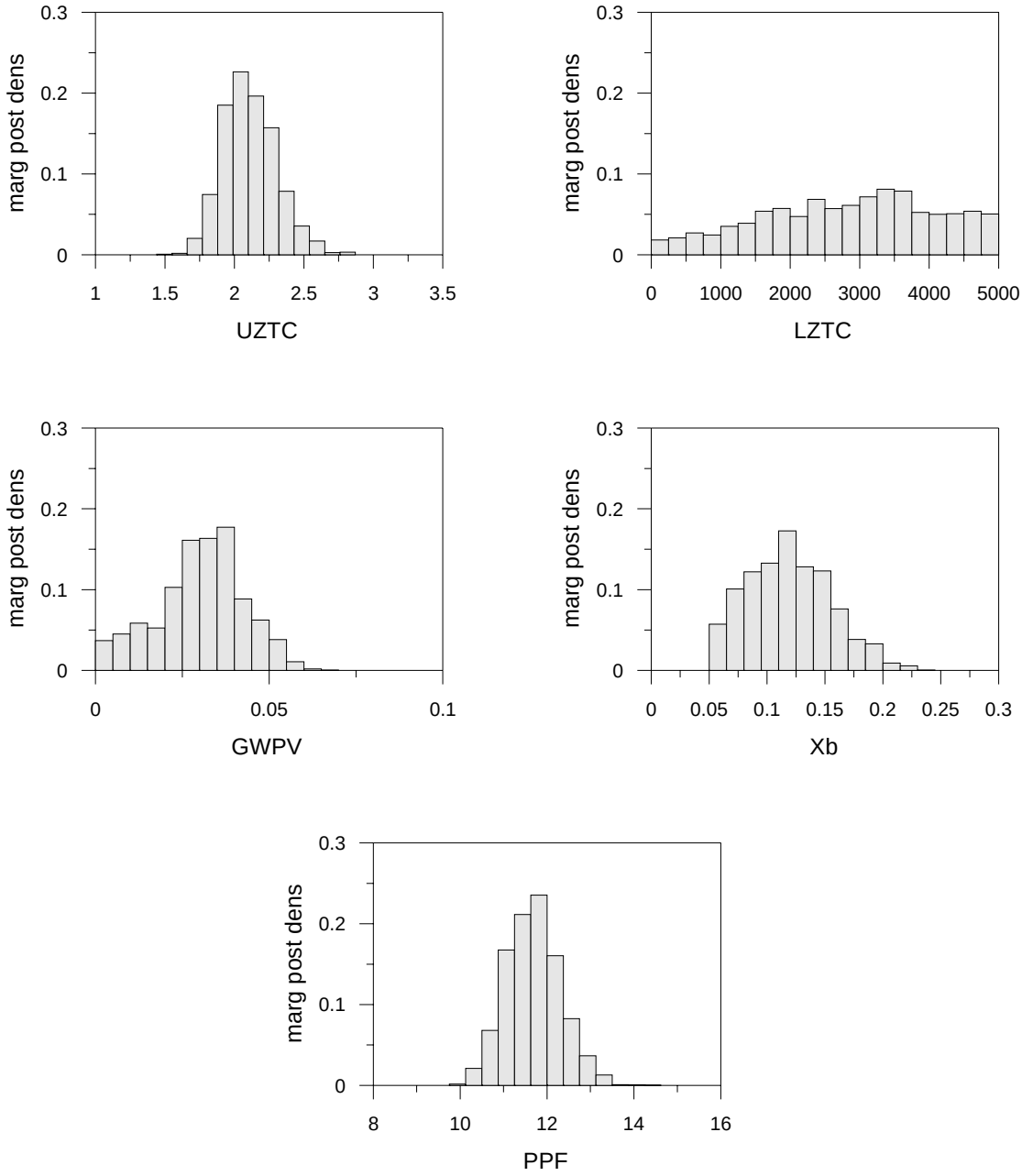

Figure 3.3. Marginal posterior probability distributions of the 5 LISFLOOD calibration parameters.

Table 3.1. Summarizing statistics of the posterior parameter distribution (optimal parameter set, posterior mean, standard deviation and correlation coefficients between the generated samples).

parameter	opt	mean	st dev	UZTC	LZTC	GWPV	Xb	PPF
UZTC	2.04	2.11	0.19	1	-0.07	0.07	0.71	-0.45
LZTC	3142	2837	1251	-	1	-0.03	-0.01	0.01
GWPV	0.03	0.03	0.01	-	-	1	0.07	0.00
Xb	0.11	0.12	0.04	-	-	-	1	-0.34
PPF	11.8	11.6	0.62	-	-	-	-	1

Figure 3.4 presents scatter plots in two dimensions of the parameter space of the 7,000 parameters sets sampled from the posterior parameter distribution. The top two plates are representative for the two parameters (LZTC and GWPV) that determine the slow groundwater response of the model. Due to the small contribution of the lower groundwater zone, these parameters show no correlation with the other calibration parameters, which is confirmed by the summarizing correlation coefficients presented in Table 3.1. The bottom three scatter plots and the corresponding correlation coefficients reveal that the parameters that affect the fast response of the model (UZTC, Xb and PPF), either through surface runoff or fast groundwater contribution, are correlated. This correlation can be explained as follows. A decrease in the value of Xb results in (i) more infiltration, hence an increase in soil moisture content and a higher flux out of the soil zone to the groundwater zone, and (ii) less surface runoff. The increased flux to the groundwater zone through infiltration can be compensated for by increasing the value of PPF, resulting in less preferential flow to the groundwater zone for the same moisture content (i.e., infiltration and preferential flow are ‘competing’ processes that recharge the upper groundwater zone). A decrease in surface runoff on the other hand is offset by smaller residence times in the upper groundwater zone, or lower values for the UZTC.

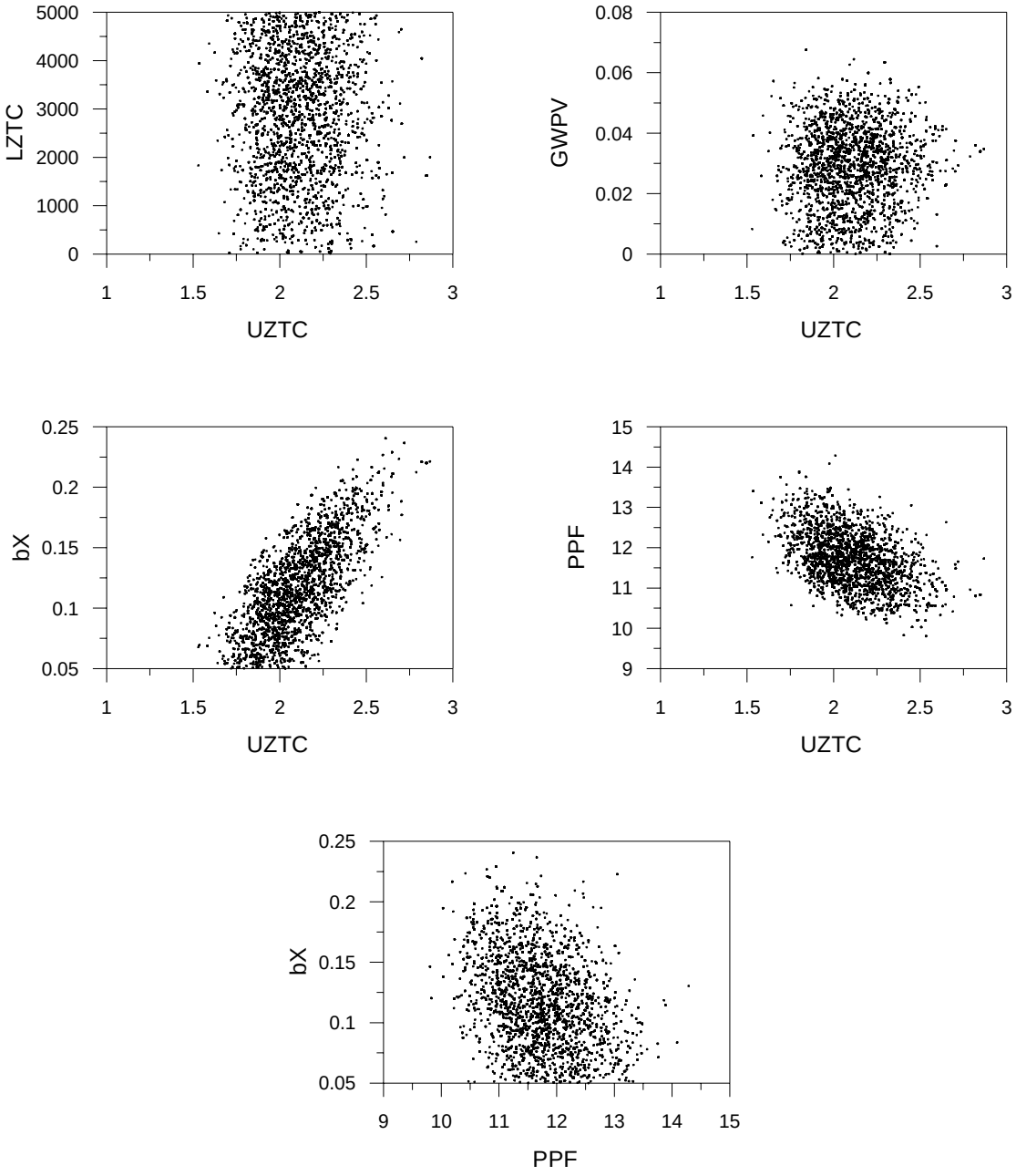

Figure 3.4. Scatter plots in 2 dimensions of parameter space of 7,000 MCMC sampled parameter sets for different combinations of parameters.

To ensure that the posterior parameter distribution adequately describes parameter uncertainty we perform some diagnostic checks on the modelling residuals. Simulations of the hydrograph were obtained by running the LISFLOOD model for 7,000 parameter combinations sampled from the posterior parameter distribution. For each simulation the transformed residuals were obtained as the difference between the Box-Cox transformed observed and simulated discharge series. The normal probability plot of the mean transformed residuals (transformed residuals averaged over the 7,000 simulations)

shown in Figure 3.5 reveals that the residuals closely conform to a normal distribution. This was confirmed by the Kolmogorov-Smirnov and Lilliefors tests at a 5% significance level. The plot of the mean transformed residuals versus the transformed predicted runoff obtained with the most likely parameter set is shown in Figure 3.6, and does not display a strong dependence of the variability of the residuals on predicted runoff. However, the plot reveals that there is a tendency for small discharges to be overestimated. Figure 3.7 presents the autocorrelation function (ACF) of the mean transformed residuals. The ACF indicates that the transformed residuals are dependent in time, which could be corrected for using an autoregressive (AR), moving average or mixed (ARMA) model for the errors. Notwithstanding we did not apply any measures to correct for autocorrelation in the residuals, which could lead to reduced estimates of the parameter uncertainty, the MCMC approach offers a powerful tool for studying parameter uncertainty.

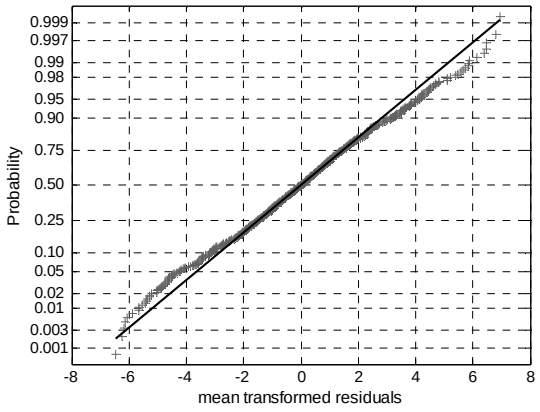

Figure 3.5. Normal probability plot for the mean transformed residuals.

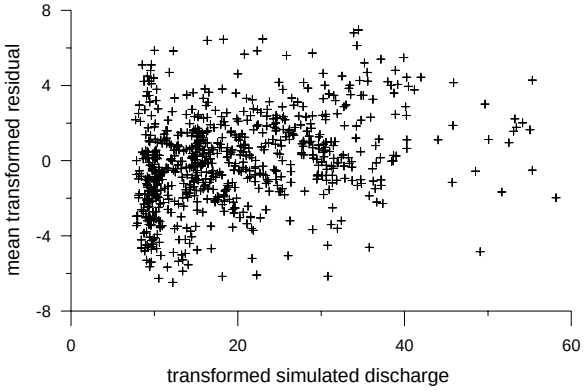

Figure 3.6. Plot of mean transformed residuals against the transformed predicted runoff obtained with the most likely parameter set.

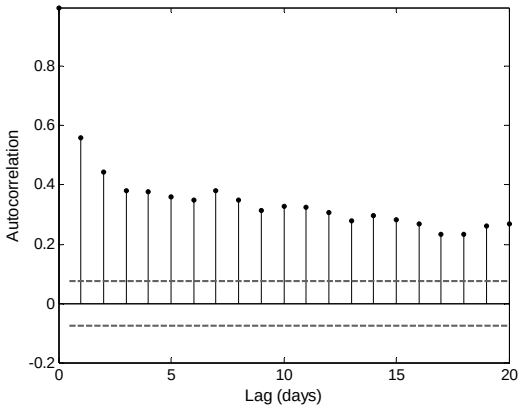

Figure 3.7. Autocorrelation function plot of the mean transformed residuals. The dashed lines depict the 95% confidence intervals about zero.

Probabilistic predictions of the hydrograph were obtained from the discharge series simulated by the LISFLOOD model for 7,000 parameter combinations sampled from the posterior parameter distribution. Results for the calibration (10/1/1993-9/30/1995) and validation (10/1/1990-9/30/1992) period are presented in Figure 3.8 and Figure 3.9, respectively. The top plates in these figure show a plot of the observed discharges (dark line), the 95% prediction uncertainty associated with only parameter uncertainty (orange shaded area), and the 95% prediction uncertainty associated with the total error in terms of modelling residuals (yellow shaded area). The latter are computed as follows. The standard deviation of the error model, which is assumed constant in the transformed space, is obtained from the RMSE between the transformed observed discharges and the transformed simulated discharges using the most likely parameter set. For each of the 7,000 simulations a constant error term equal to ±1.96*RMSE is added to the transformed discharges at each time step. The obtained prediction uncertainty limits in the transformed space are then transformed back to the original output space, which explains the varying width of the total prediction uncertainty limits with time. The bottom plates in Figure 3.8 and Figure 3.9 show the observed discharges (dark line) and prediction uncertainty expressed as a deviation from the hydrograph simulated with the most likely parameter set.

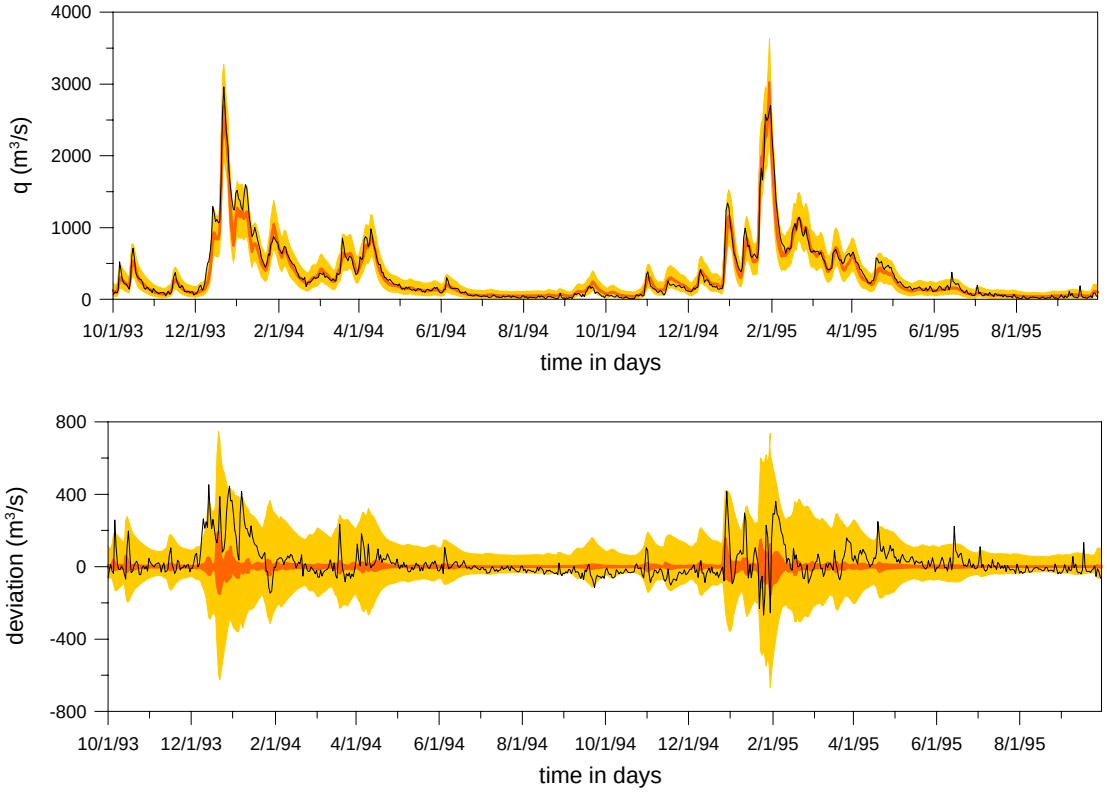

Figure 3.8 Hydrograph prediction uncertainty for the calibration period (10/1/1993-9/30/1995) period. Observed discharges are represented by the black line. The orange shaded area denotes the prediction uncertainty that results from parameter uncertainty. The yellow shaded area denotes the additional prediction uncertainty that results from model and measurement uncertainty. Top plate shows absolute values, bottom plate shows deviations from the hydrograph simulated with the most likely parameter set.

The results show that the model predictions reproduce the observed discharges reasonably well during the calibration and validation period. The noticeable over-prediction for the summers of 1991 and 1992 is likely caused by the extraction of water upstream of Borgharen, which can amount to 50 m^3/s and is not represented in the model. The 95% total prediction uncertainty bounds brackets the observations most of the time. For some periods the total prediction uncertainty is quite large, indicating that the model and/or measurement uncertainty is considerable. The 95% uncertainty region associated with parameter uncertainty is narrow and does not always bracket the observations, indicating that the model structure or the model input data may be in need of further improvement.

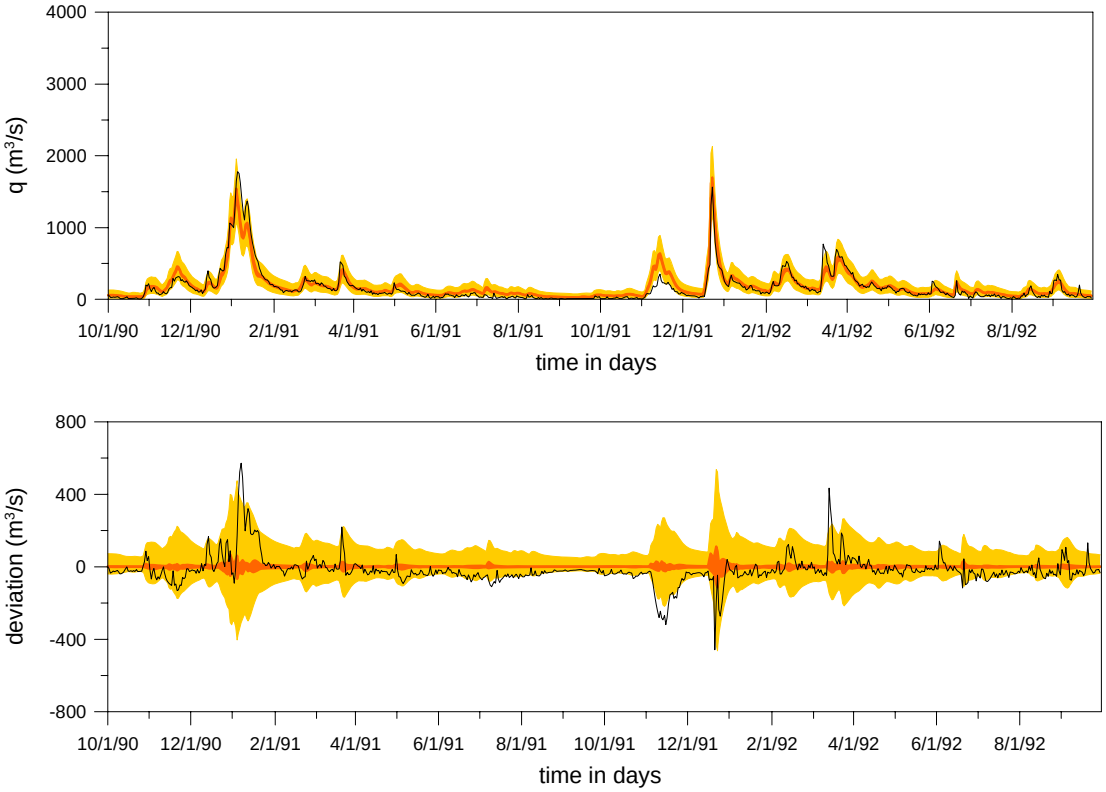

Figure 3.9. Hydrograph prediction uncertainty for the calibration period (10/1/1990-9/30/1992) period. Observed discharges are represented by the black line. The orange shaded area denotes the prediction uncertainty that results from parameter uncertainty. The yellow shaded area denotes the additional prediction uncertainty that results from model and measurement uncertainty. Top plate shows absolute values, bottom plate shows deviations from the hydrograph simulated with the most likely parameter set.

3.2. Semi-distributed calibration for the Morava catchment

The goal of this exercise is to evaluate if spatially distributing the calibration parameters within the catchment improves the predictive capabilities of the model. Results are presented for a part of the Morava catchment, covering an area of approximately 10.000 km^2. The Morava river is situated in Central Europe, with parts in Austria, the Czech Republic and the Slovak Republic, and it forms one of the most important tributaries of the Danube River. The river springs in the forested Jeseniky Mountains; further downstream it flows through wide valleys and plains. The main part of the Morava River has typically lowland character with small slopes and alluvial floodplains on both sides. The Morava basin has a typical continental climate with an annual precipitation of about 640 mm.

Calibration Strategy 1:

Uniform parameters, calibration against discharge at the outlet of the catchment (Straznice)

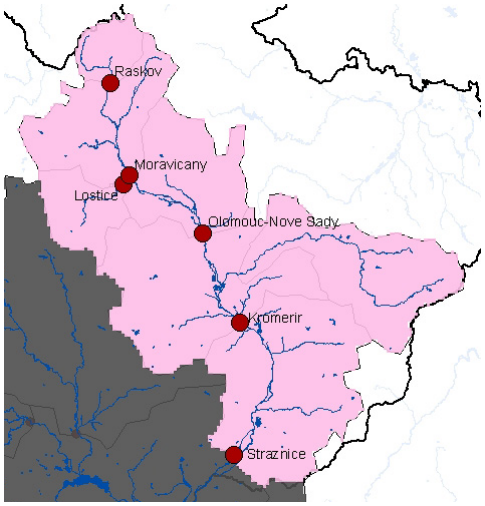

Calibration Strategy 2:

Uniform parameters, calibration against discharge at the outlet of the catchment (Straznice) and the internal discharge stations.

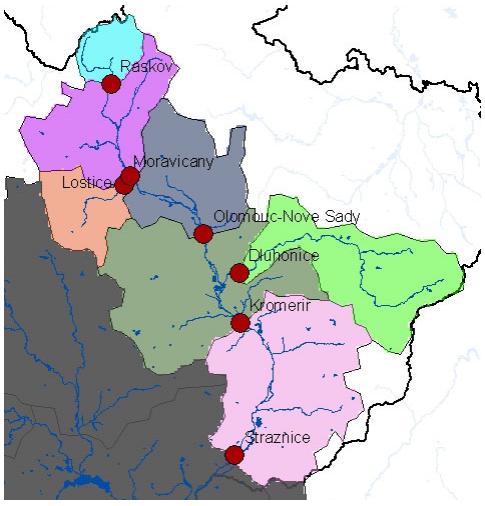

Calibration Strategy 3:

Semi-distributed parameters (uniform within each of the subcatchments), calibration against discharge at the outlet of the corresponding subcatchment.

Figure 3.10. Overview of the 3 calibration strategies adopted for the Morava catchment.

To evaluate the effect of semi-distributed parameters, three different calibration strategies are adopted, as depicted in Figure 3.10. In the first strategy, the calibration parameters are uniformly distributed over the area of interest and are calibrated against the discharge at the outlet of the catchment (Straznice). The parameters are also uniformly distributed in the second strategy, but they are calibrated against the discharge at Straznice and the internal discharge stations. In the third strategy a semi-distributed approach is adopted. Starting from upstream, parameters in each subcatchment are calibrated against the observed discharges at the outlet of the subcatchment. In order not to propagate upstream errors in the calibration process, observed discharges at upstream catchment outlets are used as inflow when calibrating downstream subcatchments.

Results for the different gauging stations of the subcatchments are presented in Figures 3.11 to 3.17. The plates in these figures represent the observed discharges and the hydrograph prediction uncertainty as a deviation from the hydrograph simulated with the most likely parameter set. The dark line represents the difference between the observed hydrograph and the hydrograph simulated with the most likely parameter set. The orange shaded area represents the uncertainty in the predictions due to uncertainty in the parameters, whereas the yellow shaded area represents the total uncertainty in the predictions (due to parameter, model and measurement uncertainty). The top plate in each figure corresponds to the first calibration strategy. The middle plates represent the second calibration strategy, and the bottom plates show results of the semi-distributed approach. On the right of each plate, based on the simulation with the most likely parameter set, values are presented of the following 3 statistical measures

$$\mathrm{EF} = 1 - \frac{\sum_{t=1}^{n} (Q_{obs,t} - Q_{sim,t})^2}{\sum_{t=1}^{n} (Q_{obs,t} - \overline{Q}_{obs})^2} \tag{3.1}$$

$$\mathrm{bias} = \frac{\sum_{t=1}^{n} | Q_{obs,t} - Q_{sim,t} |}{\sum_{t=1}^{n} Q_{obs,t}} \tag{3.2}$$

$$R^2 = \left\{ \frac{\sum_{t=1}^{n} (Q_{obs,t} - \overline{Q}_{obs})(Q_{sim,t} - \overline{Q}_{sim})}{\sum_{t=1}^{n} (Q_{obs,t} - \overline{Q}_{obs})^{0.5} (Q_{obs,t} - Q_{sim,t})^{0.5}} \right\}^2 \quad (3.3)$$

The coefficient of efficiency E is the ratio of the mean square error to the variance in the observed data, substracted from unity. It ranges from minus infinity to 1.0, with higher values indicating a better agreement. The coefficient of determination R^2 describes the proportion of the total variance in the observed data that can be explained by the model. It ranges from 0.0 to 1.0, with higher values indicating better agreement. Because of the squared differences E and R^2 are overly sensitive to extreme values. The bias coefficient reflects the absolute simulation error relative to the observations. It varies between 0.0 and infinity, with lower values indicating a better agreement.

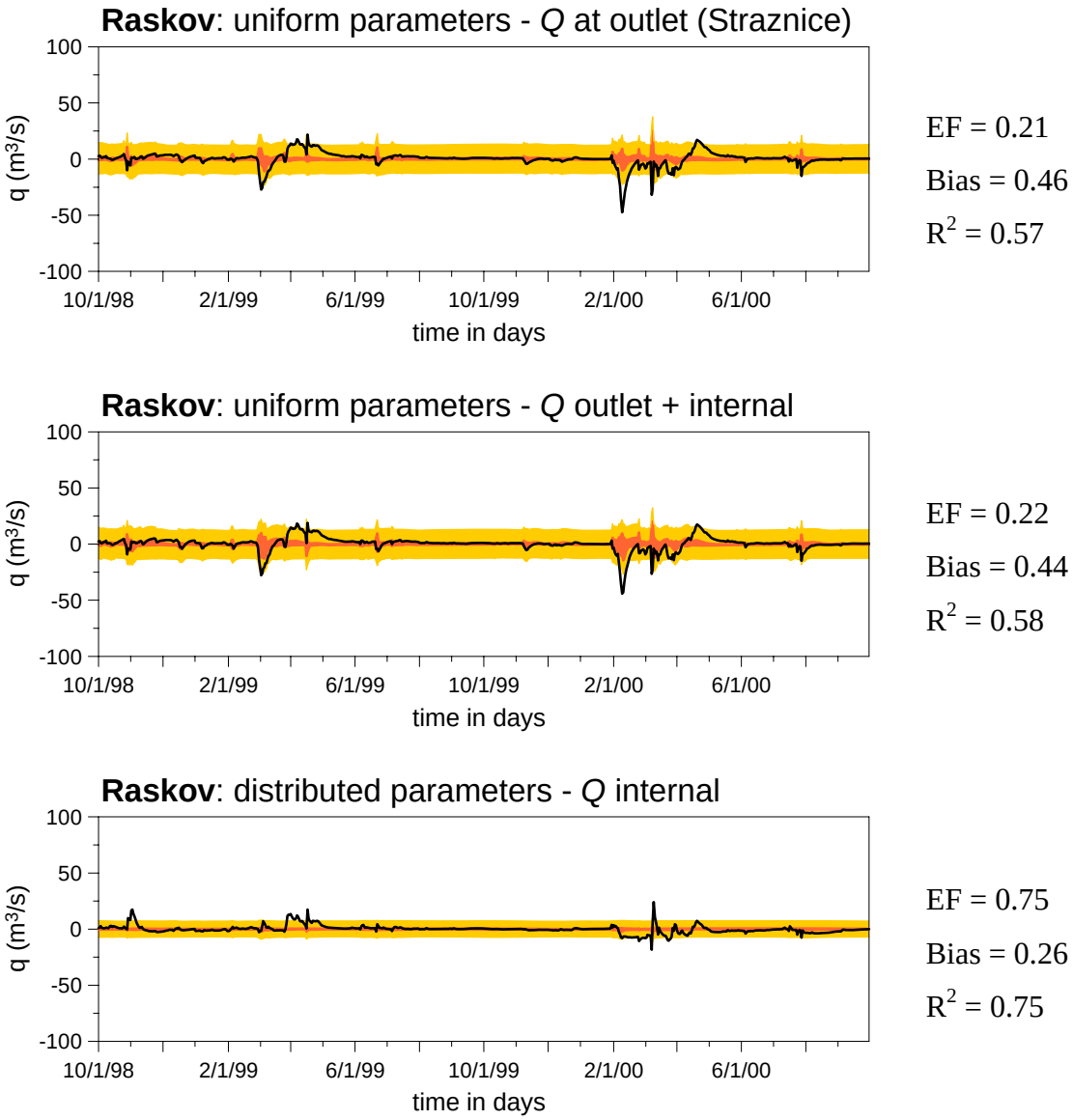

Figure 3.11. Hydrograph prediction uncertainty associated with the most likely parameter set derived using SCEM-UA for Raskov. Observed discharges are represented by the black line. The orange shaded area denotes the prediction uncertainty that results from parameter uncertainty. The yellow shaded area denotes the additional prediction uncertainty that results from input, model and measurement uncertainty.

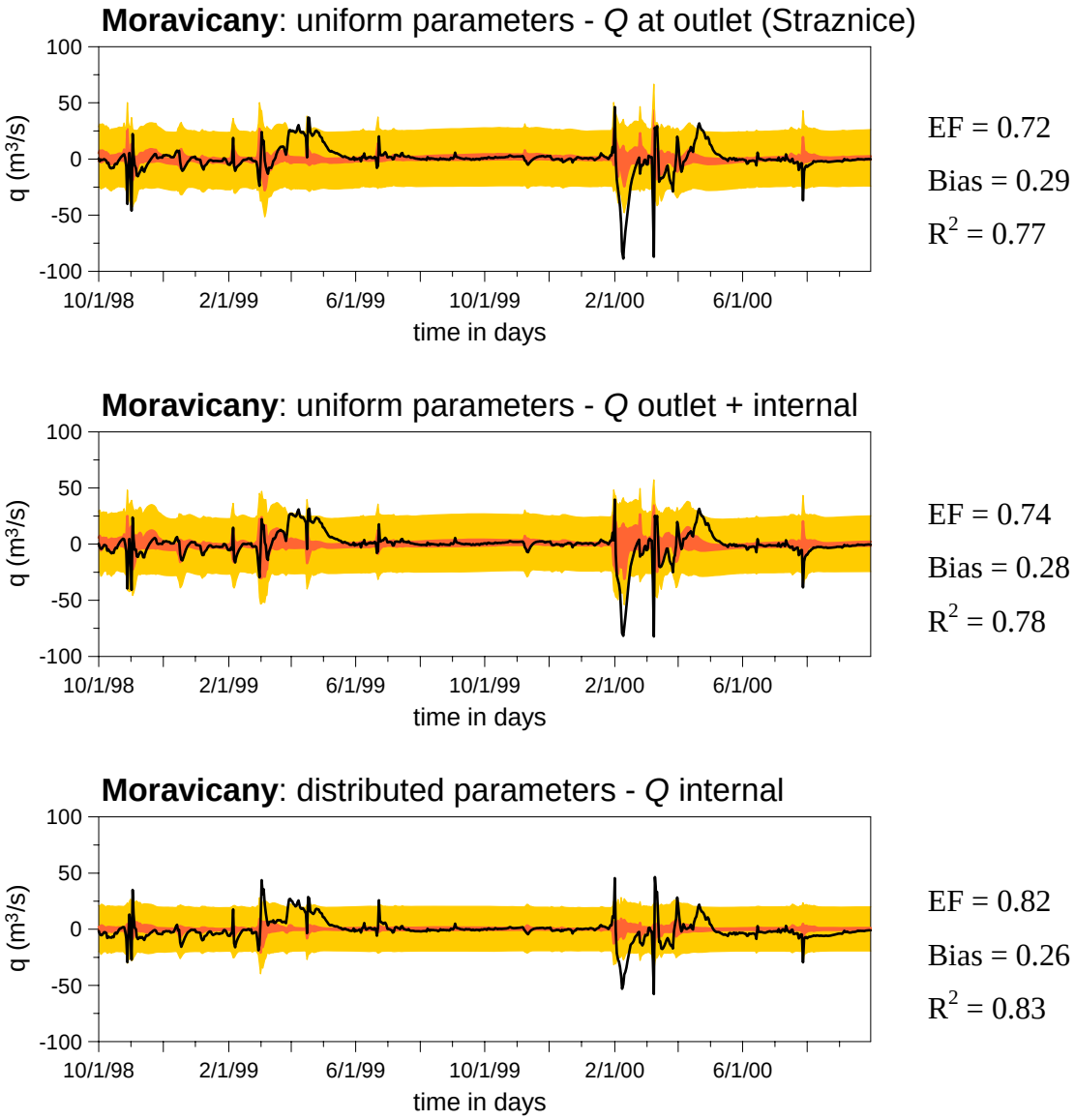

Figure 3.12. Hydrograph prediction uncertainty associated with the most likely parameter set derived using SCEM-UA for Moravicany. Observed discharges are represented by the black line. The orange shaded area denotes the prediction uncertainty that results from parameter uncertainty. The yellow shaded area denotes the additional prediction uncertainty that results from input, model and measurement uncertainty.

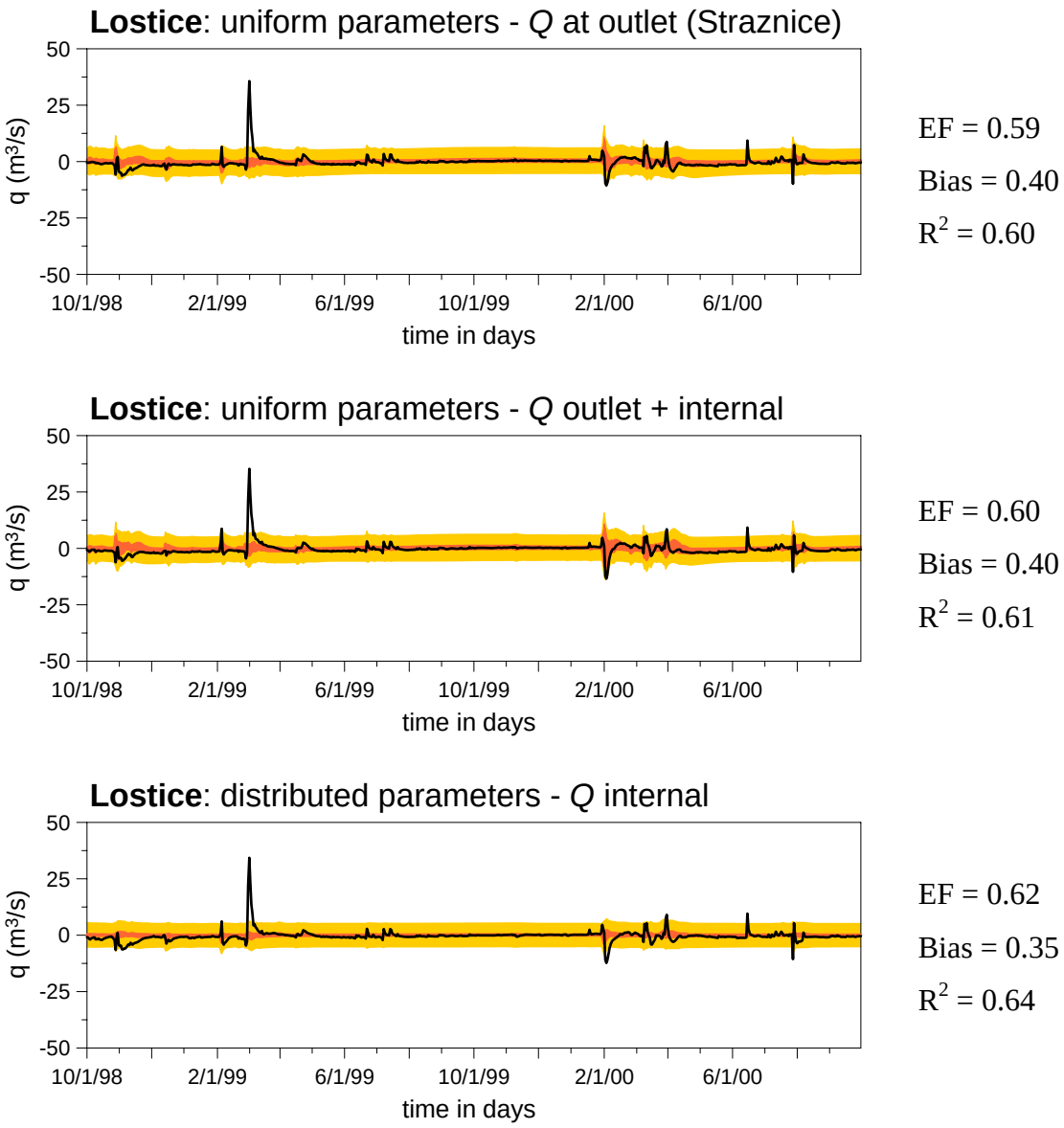

Figure 3.13. Hydrograph prediction uncertainty associated with the most likely parameter set derived using SCEM-UA for Lostice. Observed discharges are represented by the black line. The orange shaded area denotes the prediction uncertainty that results from parameter uncertainty. The yellow shaded area denotes the additional prediction uncertainty that results from input, model and measurement uncertainty.

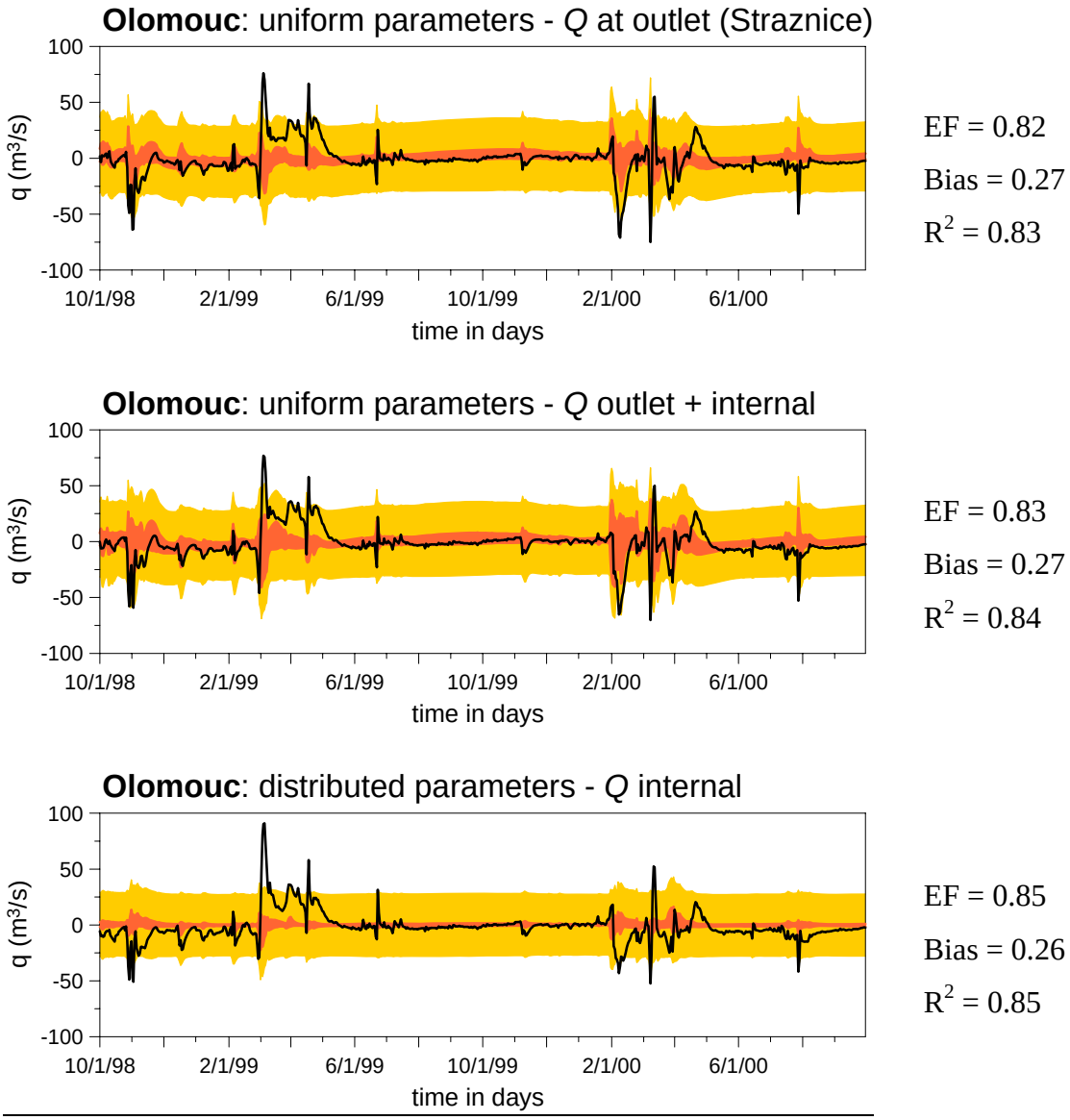

Figure 3.14. Hydrograph prediction uncertainty associated with the most likely parameter set derived using SCEM-UA for Olomouc. Observed discharges are represented by the black line. The orange shaded area denotes the prediction uncertainty that results from parameter uncertainty. The yellow shaded area denotes the additional prediction uncertainty that results from input, model and measurement uncertainty.

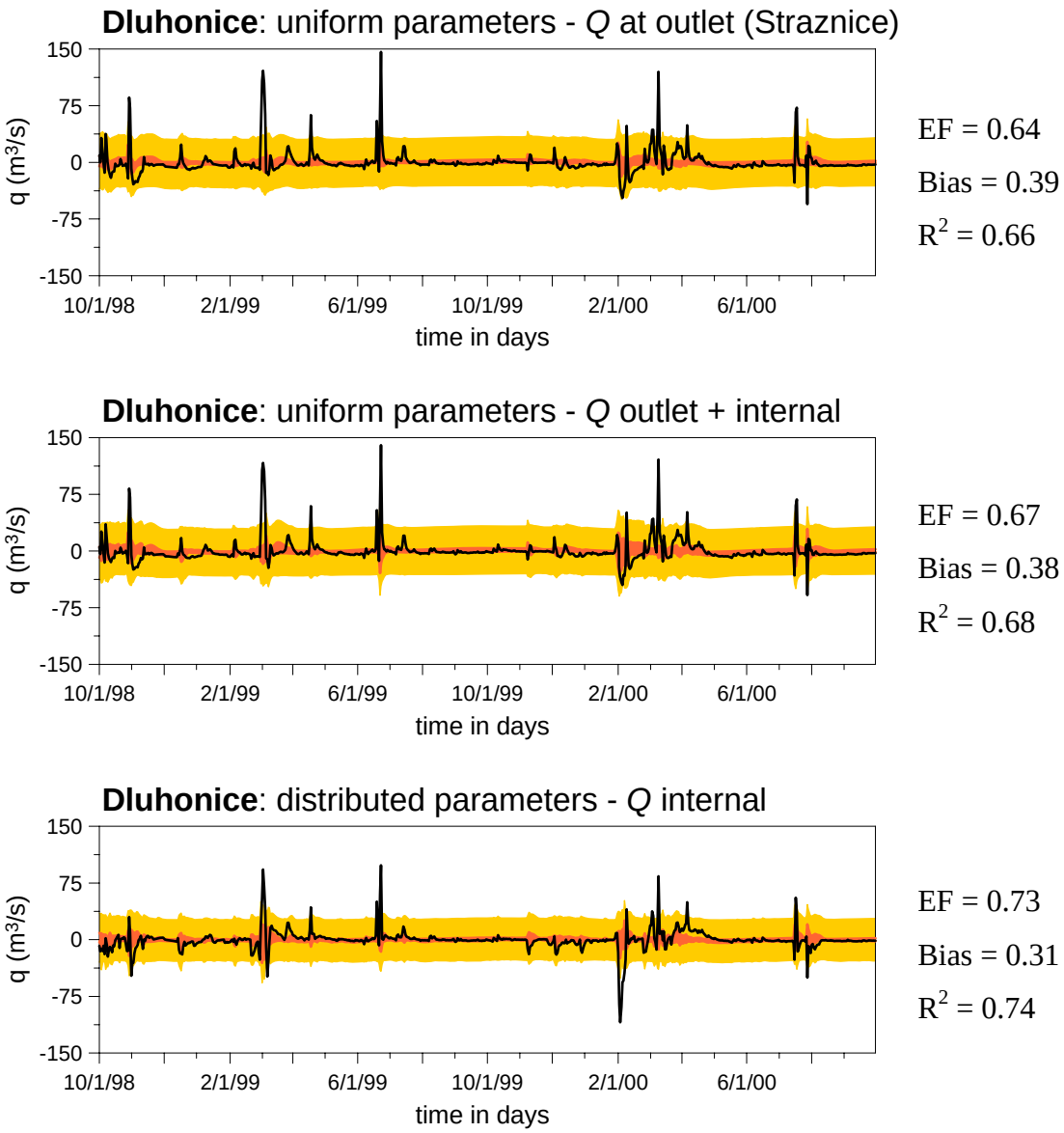

Figure 3.15. Hydrograph prediction uncertainty associated with the most likely parameter set derived using SCEM-UA for Dluhonice. Observed discharges are represented by the black line. The orange shaded area denotes the prediction uncertainty that results from parameter uncertainty. The yellow shaded area denotes the additional prediction uncertainty that results from input, model and measurement uncertainty.

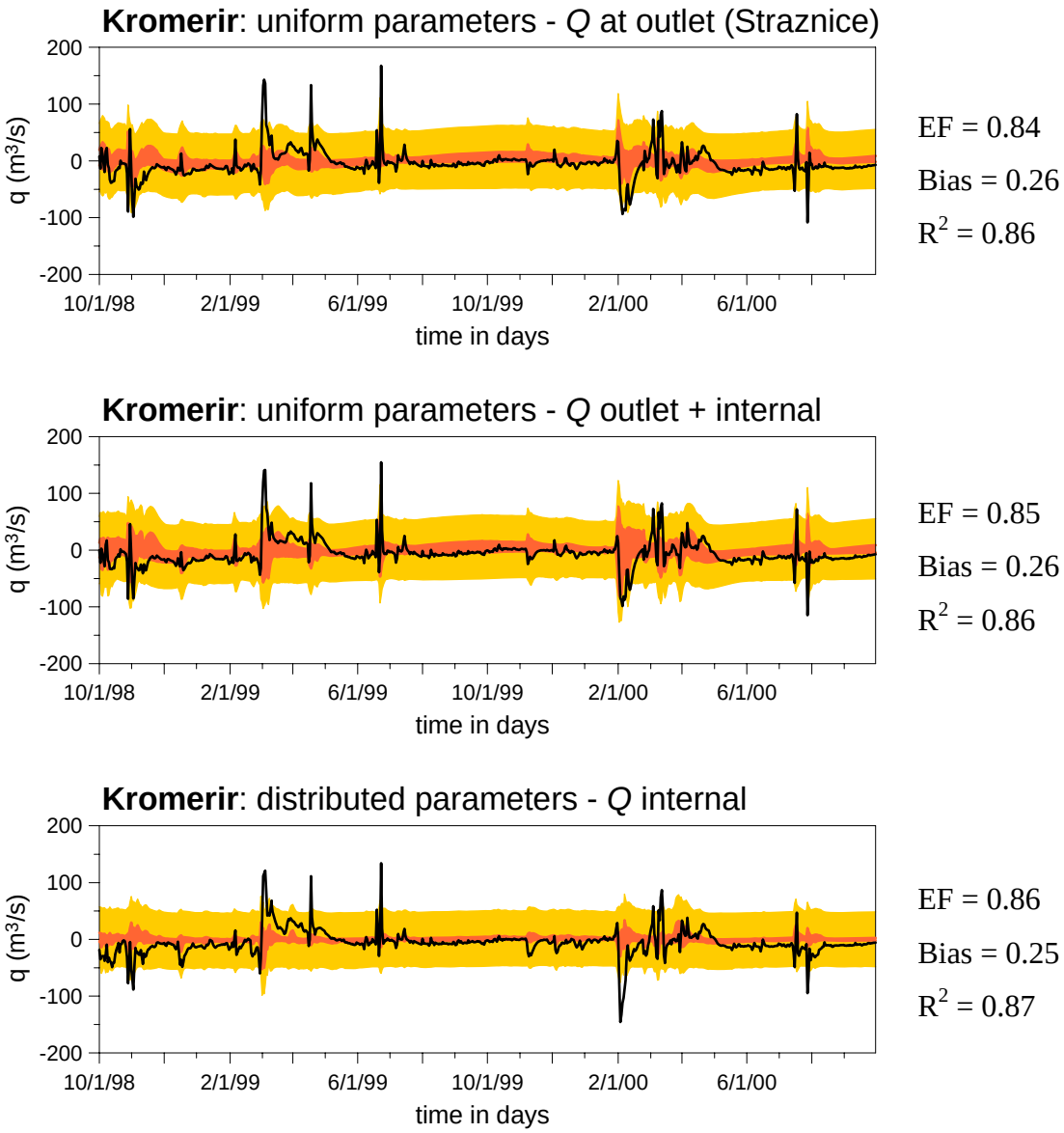

Figure 3.16. Hydrograph prediction uncertainty associated with the most likely parameter set derived using SCEM-UA for Kromerir. Observed discharges are represented by the black line. The orange shaded area denotes the prediction uncertainty that results from parameter uncertainty. The yellow shaded area denotes the additional prediction uncertainty that results from input, model and measurement uncertainty.

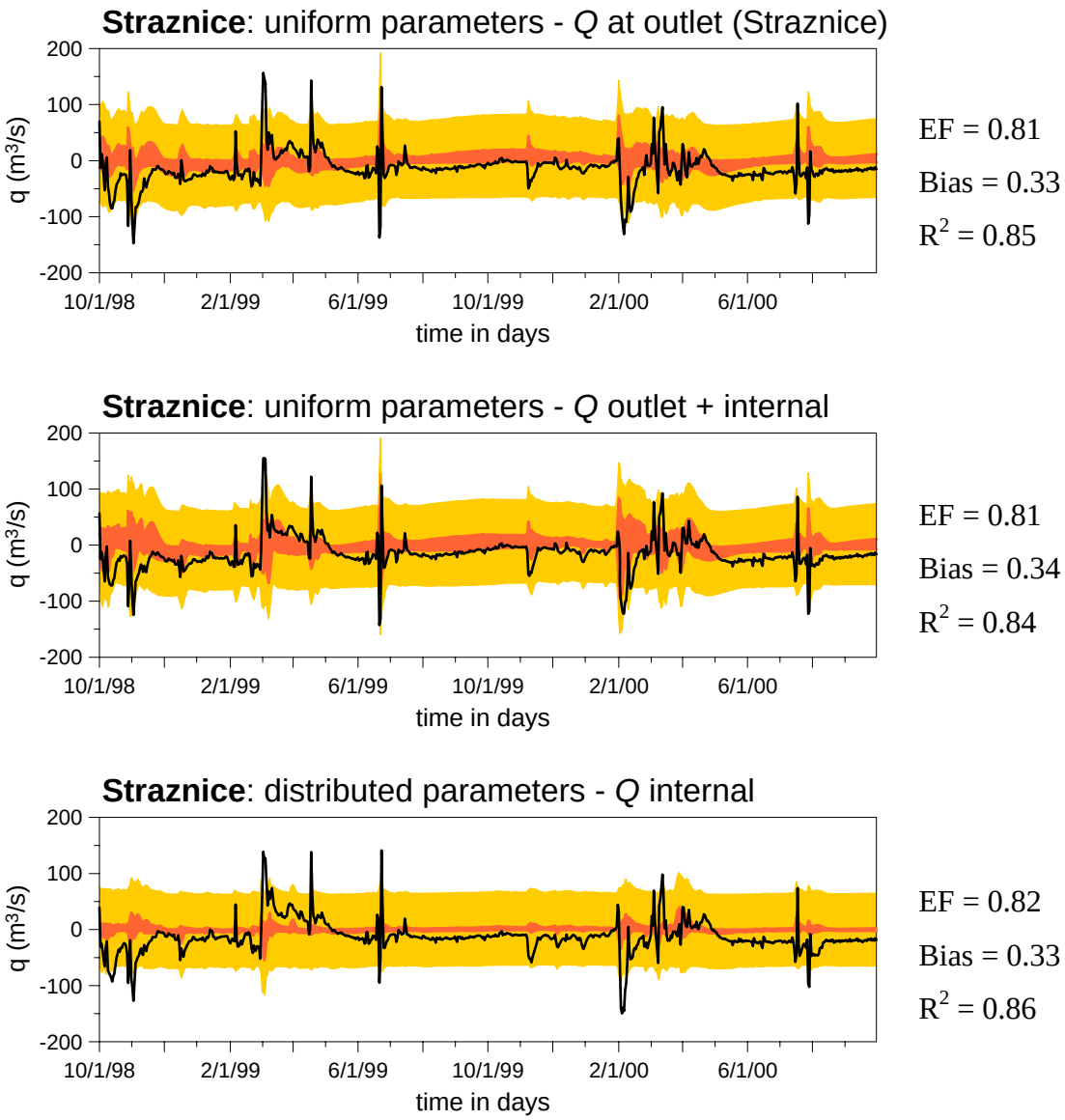

Figure 3.17. Hydrograph prediction uncertainty associated with the most likely parameter set derived using SCEM-UA for Straznice. Observed discharges are represented by the black line. The orange shaded area denotes the prediction uncertainty that results from parameter uncertainty. The yellow shaded area denotes the additional prediction uncertainty that results from input, model and measurement uncertainty.

From the above figures, the following findings should be noted. First, the calibration of uniform parameter values against discharges at the catchment outlet results in good reproductions of the hydrograph at the downstream stations, but inferior fits are obtained for more upstream subcatchments. Including internal discharge observations in the objective function slightly improves the results for all subcatchments, expect for the most downstream one. This can be attributed to the fact that the uniform parameter

values also have to reproduce internal observations, and not only those at the outlet. The semi-distributed approach considerably improves the predictions, especially in the upstream catchments. Further downstream, improvements are less pronounced, largely because the uniform approaches yield good results in these areas.

A second important finding is the observed changes in parameter uncertainty between the different calibration strategies. Parameter uncertainty (and consequently the corresponding predictive uncertainty) is smallest for the semi-distributed approach. This is because calibration of the sub-catchments individually results in an improved identification of the ranges of parameter attraction, which can vary considerably among the different sub-catchments. The uniform approaches result in more parameter (and corresponding predictive) uncertainty because uniform parameter values are less able to represent the varying hydrological properties in the different subcatchments, and therefore are less well identifiable. Parameter uncertainty is largest for the uniform parameter values calibrated against the observations at the outlet and the internal discharge stations (strategy 2). This is because the uniform parameter values also need to reproduce internal observations. Uniform parameter values that reproduce discharges at catchment outlet well may be in conflict with internal observations, which results in a less pronounced region of attraction.

The semi-distributed approach also results in a considerable reduction in the total uncertainty with respect to the uniform approaches. Since the input and measurement uncertainty do not differ between the calibration strategies, the increase in total uncertainty can be attributed to an increase in parameter and model uncertainty. It should be stressed that the increase in model uncertainty here reflects the change in parameterisation, i.e., uniform instead of semi-distributed parameter values, which can be assumed to be a less correct representation of the true unknown distribution of the hydrological properties.

4. Conclusions

The current LISFLOOD model has been calibrated for several test catchments using the automatic Shuffled Complex Evolution Metropolis-UA optimization algorithm. The results indicate that SCEM-UA is able in most cases to identify the optimal parameter values and to infer the posterior parameter distribution that reflects the residual parameter uncertainty. Results of a semi-distributed approach also show the clear need to spatially vary the calibration parameters, especially in large catchments characterized by spatially varying hydrological processes and responses. Other advantages are the less subjective nature and a more exhaustive exploration of the parameter space compared to manual calibration.

The drawback of SCEM-UA is that the objective function is based on the sum of squared errors, which implies certain assumptions on the modelling residuals (but allows a formal estimation of the parameter and total uncertainty). Whenever the underlying assumptions are not met, a transformation of the observed and simulated errors can be applied. However, this is not a straightforward exercise, and somewhat hampers the application of the technique on a routinely basis. Another limitation of this technique, and of single-objective methods in general, is that the assessment of fit is compacted into one single measure (e.g., least squares), which may not capture all the aspects of a time series of observations one is interested in.

5. Further work

Calibration of the LISFLOOD model for all catchments in Europe is an enormous task, and will require much more time and effort. It will be closely linked to further improvements in the model structure and input data. Important issues that need to be addressed are:

- Include more parameters in the calibration procedure (e.g., parameters from snow routine).
- Employ multi-objective optimization tools that include different measures of fit favouring different aspects of discharge series to arrive at more robust parameter estimates.
- Separate the individual effects of input, parameter and model uncertainty.
- Analyze the effect of the different sources of hydrological uncertainty on probabilistic flood forecasts.
- What is the robustness of optimal parameters (and parameter uncertainty) in relation to temporal and spatial resolution, i.e., are optimal parameters (and associated parameter uncertainty) transferable across temporal and spatial scales?

Can regionalization techniques be applied to transfer parameter values to ungauged catchments?

References

Box G.E.P., and G.C. Tiao, 1973. Bayesian inference in statistical analysis, Addison-Wesley-Longman, Reading, MA.

De Roo, A.P.J., C.G. Wesseling, and W.P.A. Van Deurzen, 2000. Physically-based river basin modelling within a GIS: the LISFLOOD model. Hydrological Processes, 14, 1981-1992.

De Roo, A.P.J., M. Odijk, G. Schmuck, E. Koster, and A. Lucieer, 2001. Assessing the effects of land use changes on floods in the Meuse and Oder catchment. Physics and Chemistry of the Earth (B), 26(7-8), 593-599.

Eaton, J.W., 1998. Web: http://www.octave.org/, University of Wisconsin, Department of Chemical Engineering, Madison WI 53719.

Eaton, J.W., 2001. Octave: Past, Present and Future. Proceedings of the 2nd international workshop on distributed statistical computing, March 2001, Vienna, Austria.

European Environment Agency, 2000. The European Topic Centre on Terrestrial Environment: Corine land cover raster database 2000 - 100m.

Feyen, L., B. Ó Nualláin, J.A. Vrugt, J. van der Knijff, and A. De Roo, 2005a. Automatic parameter identification for a rainfall-runoff model within the European Flood Alert System, In: Proceedings of the International Conference on Innovation, advances and implementation of flood forecasting technology, Tromsø, Norway, October 17-19, 2005.

Feyen, L., M. Kalas, J.A. Vrugt, J. van der Knijff, and A. De Roo, 2005b. Parameter identification and uncertainty estimation for a spatially distributed rainfall-runoff model using global optimization, Eos Trans. AGU, 86(52), Fall Meet. Suppl., Abstract H41G-04.

Feyen, L., J.A. Vrugt, B. Ó Nualláin, J. van der Knijff, and A. De Roo, 2006a. Parameter optimisation and uncertainty assessment for large-scale streamflow simulation with the LISFLOOD model, In review, Journal of Hydrology.

Feyen, L., M. Kalas, J.A. Vrugt, J. van der Knijff, and A. De Roo, 2006b. The value of semi-distributed parameters for large-scale streamflow simulation, Manuscript in preparation, to be submitted to Water Resources Research.

Fernández, J., A. Cañas, A.F. Díaz, J. González, J. Ortega, and A. Prieto, 2003. Performance of Message-Passing MATLAB Toolboxes. 5th International

conference on high performance computing in computational sciences, Lecture notes in computer science, 2565, 228-241.

Fernández, J., M. Anguita, S. Mota, A. Cañas, E. Ortigosa, and F.J. Rojas, 2004. MPI Toolbox for Octave. Proceedings of the 6th international conference on high performance computing for computational science, June 2004, Valencia, Spain.

Gelman, A., D.B. Rubin, 1992. Inference from iterative simulation using multiple sequences. Statistical Science, 7(4), 457-472.

Hastings, W.K., 1970. Monte Carlo sampling methods using Markov Chains and their applications, Biometrika, 57, 97-109.

Hiederer, R. and A. de Roo, 2003. A European flow network and catchment data set. Report of the European Commission, Joint Research Centre, EUR 20703 EN.

King D., J. Daroussin, and R. Tavernier, 1994. Development of a soil geographical database from the soil map of the European Communities. Catena, 21, 37-56.

Kuczera, 1983. Improved parameter inference in catchment models, 1. Evaluating parameter uncertainty. Water Resources Research, 19(5), 1151-1162.

Metropolis, N., A.W. Rosenbluth, M.N. Rosenbluth, A.H. Teller, E. Teller, 1953. Equations of state calculations by fast computing machines. Journal of Chemical Physics, 21, 1087-1091.

Sorooshian, S., and J.A. Dracup, 1980. Stochastic parameter estimation procedures for hydrologic rainfall-runoff models: correlated and heteroscedastic error cases. Water Resources Research, 16(2), 430-442.

Vrugt, J.A., H.V. Gupta, W. Bouten, and S. Sorooshian, 2003. A Shuffled Complex Evolution Metropolis algorithm for optimization and uncertainty assessment of hydrologic parameter estimation. Water Resources Research, 39(8), 1201, doi:10.1029/2002WR001642.

Vrugt, J.A., G.H. Schoups, J.W. Hopmans, C.H. Young, W. Wallender, T. Harter, and W. Bouten, 2004. Inverse modeling of largescale spatially distributed vadose zone properties using global optimization, Water Resources Research, 40(6), W06503, doi:10.1029/2003WR002706.

Vrugt, J.A., B.Ó Nualláin, B.A. Robinson, W. Bouten, S.C. Dekker, and P.M.A. Sloot, 2005. Application of parallel computing to stochastic parameter estimation in environmental models, Computers & Geosciences (in press).

Wösten, J.H.M., A. Lilly, A. Nemes, and C. Le Bas, 1999. Development and use of a database of hydraulic properties of European soils. Geoderma, 90(3-4), 169-185.

Zhao, R.J. and X.R. Liu, 1995. The Xinanjiang model. In: Singh, V.P. (Ed.), Computer Models of Watershed Hydrology, Water Resources Publications, Littleton, Colorado, 215-232.

EUROPEAN COMMISSION
DIRECTORATE-GENERAL
Joint Research Centre

The mission of the Joint Research Centre is to provide customer-driven scientific and technical support for the conception, development, implementation and monitoring of European Union policies. As a service of the European Commission, the JRC functions as a reference centre of science and technology for the Community. Close to the policy-making process, it serves the common interest of the Member States, while being independent of special interests, whether private or national.

Publications Office
Publications.eu.int